

## Inner Molecular Rings in Barred Galaxies: BIMA SONG CO Observations

Michael W. Regan<sup>1,2</sup>, Kartik Sheth<sup>2,3,4</sup>, Peter J. Teuben<sup>3</sup>, Stuart N. Vogel<sup>3</sup>,

### ABSTRACT

Although inner star-forming rings are common in optical images of barred spiral galaxies, observational evidence for the accompanying molecular gas has been scarce. In this paper we present images of molecular inner rings, traced using the CO (1–0) emission line, from the Berkeley-Illinois-Maryland-Association Survey of Nearby Galaxies (BIMA SONG). We detect inner ring CO emission from all five SONG barred galaxies classified as inner ring (type (r)). We also examine the seven SONG barred galaxies classified as inner spiral (type (s)); in one of these, NGC 3627, we find morphological and kinematic evidence for a molecular inner ring. Inner ring galaxies have been classified as such based on optical images, which emphasize recent star formation. We consider the possibility that there may exist inner rings in which star formation efficiency is not enhanced. However, we find that in NGC 3627 the inner ring star formation efficiency is enhanced relative to most other regions in that galaxy. We note that the SONG (r) galaxies have a paucity of CO and H $\alpha$  emission interior to the inner ring (except near the nucleus), while NGC 3627 has relatively bright bar CO and H $\alpha$  emission; we suggest that galaxies with inner rings such as NGC 3627 may be misclassified if there are significant amounts of gas and star formation in the bar.

---

<sup>1</sup>Space Telescope Science Institute, 3700 San Martin Drive, Baltimore, MD 21218, mregan@stsci.edu

<sup>2</sup>Visiting Astronomer, Kitt Peak National Observatory, National Optical Astronomy Observatories, which are operated by the Association of Universities for Research in Astronomy, Inc. (AURA) under cooperative agreement with the National Science Foundation

<sup>3</sup>Department of Astronomy, University of Maryland, College Park, MD 20742

<sup>4</sup>Division of Mathematics & Physical Sciences, California Institute of Technology, Pasadena, CA, 91125

## 1. Introduction

Rings of star formation are a common hallmark of early to intermediate Hubble type barred spiral galaxies (Buta & Combes 1996). The general view is that gas collects due to gas dissipation in rings located at various resonances, driven by torques from non-axisymmetric structures such as bars (Schwarz 1984; Combes & Gerin 1985; Byrd et al. 1994; Buta & Combes 1996). Numerous studies indicate that most known rings are sites of enhanced star formation, implying that star formation is triggered in these rings (Buta & Combes 1996). Although, without a comparison between the gas in the rings and the star formation rate, it may be that rings are just locations with more fuel for star formation. Consequently, rings are important diagnostic tools for understanding galaxy dynamics and evolution.

Rings are typically classified into three major categories (Buta 1986): circumnuclear, inner, and outer rings. Circumnuclear rings are located well interior to the bar, generally within a kpc of the nucleus. Inner rings circumscribe the ends of the stellar bar, and are typically elongated parallel to the bar. Outer rings are larger, more diffuse features located well outside the bar regions, and generally elongated perpendicular to the bar. Many studies link circumnuclear, inner, and outer rings to the inner Lindblad resonance (ILR), ultra-harmonic (also known as 4:1) resonance (UHR), and outer Lindblad resonance (OLR), respectively (Buta & Combes 1996). The timescale for ring formation varies from  $5 \times 10^9$  years for the outer rings to only a few  $\times 10^7$  years for the nuclear rings (Buta & Combes 1996). Hence the presence and absence of the different ring structures can constrain the evolutionary timescale of the galactic disk and its components, e.g., bars and spiral arms. Moreover since rings may be associated with different resonances, the radii of the rings, with knowledge of the rotation curve, can place constraints on the pattern speed of the bar.

Circumnuclear rings have prodigious star formation and are most prominent in blue light (Barth et al. 1998); the associated gas is generally not in a ring morphology (Kenney et al. 1992; Sheth 2001). Inner rings are also identified almost exclusively from optical studies tracing recent star formation, such as blue light excesses or  $H\alpha$  emission. Similar to circumnuclear rings, inner rings are commonly thought to be regions where star formation is triggered and enhanced (Buta & Combes 1996). However, these conclusions are based on samples in which inner rings have been identified (i.e. selected) on the basis of excess star formation in a ring. It would therefore be useful to investigate whether there is a population of inner rings which may have remained undiscovered because the star formation is not sufficiently remarkable for the ring to stand out in the optical. Such rings might be discovered by observing the CO 1–0 emission that traces molecular gas. With an unbiased sample, the question of whether star formation is enhanced in inner rings can be properly addressed.

Following up on the NRO-OVRO CO survey of the nuclei of galaxies Sakamoto et al. (1999), Sakamoto, Baker, & Scoville (2000) identified a molecular inner ring in NGC 5005. However, few studies to date have had the capability to detect molecular rings. The problem is that at the distance of most barred galaxies, inner rings require high (i.e. interferometric) angular resolution to clearly resolve the inner rings from brighter CO features such as circumnuclear regions, bar ends, and spiral arms. However, the inner rings lie outside the primary beam of most interferometric studies, which have generally concentrated on the nuclear region. Even when larger regions are mosaiced, the spatial dynamic range has been inadequate to detect inner rings, which, as noted, are fainter than many other features in barred spirals. This situation has now changed with the BIMA CO Survey of Nearby Galaxies (SONG) (Regan et al. 2001). With BIMA SONG, the disks of 44 nearby spiral galaxies have been mosaiced with high spatial dynamic range.

## 2. Sample Selection and Observations

As described in Regan et al. (2001), the 44 BIMA SONG sample includes all galaxies except M33 which have Hubble types between Sa and Sd, recessional velocity less than  $2000 \text{ km s}^{-1}$ , inclination  $< 70^\circ$ , declination  $> -20^\circ$ , and  $M_B$  brighter than 11.0. Of the 29 SONG galaxies classified as barred (SB or SAB), five have the (r) classification indicating an inner ring, and seven have the (s) classification indicating spiral arms and the absence of an inner ring; the remaining 17 have the (rs) classification indicating a pseudo-ring or partial ring (de Vaucouleurs & Buta 1980; Buta & de Vaucouleurs 1983; Buta 1986).

The observational techniques and data reduction procedures for the CO 1–0 observations of the BIMA SONG galaxies are described in Regan et al. (2001). Summarizing, the galaxies were observed with the 10-element Berkeley-Illinois-Maryland Association (BIMA) millimeter interferometer (Welch et al. 1996). Nine of the dozen galaxies discussed in this paper were observed with a 7-field hexagonal mosaic with a spacing of  $44''$ , which gives a half-power field of view of about  $190''$ . For NGC 3627, we observed additional fields to cover a larger area. NGC 3726 and NGC 4490 were observed with a single pointing, which yields a half-power field of view of about  $100''$ . The angular resolution was typically  $6''$ . For NGC 3351 and NGC 3627, we also obtained on-the-fly observations of CO 1–0 with the NRAO 12-m single-dish telescope<sup>5</sup> and included this data in the maps using a linear mosaic technique. Initial velocity-integrated CO intensity maps were derived using the technique

---

<sup>5</sup>The National Radio Astronomy Observatory is operated by the Associated Universities, Inc., under cooperative agreement with the National Science Foundation.

described in Regan et al. (2001); CO velocity files were obtained using a similar technique. This technique detected most of the emission presented. To improve the signal to noise ratio we fit rotation curves to these velocities and generated new velocity-integrated maps by limiting the velocity range in areas of weak emission to velocities within  $\pm 50 \text{ km s}^{-1}$  of the velocity predicted by the rotation model.

As part of the SONG study, parallel observations in other wavebands were obtained. In this paper we show R band and  $\text{H}\alpha$  images of NGC 3344, NGC 3351, NGC 3627, and NGC 3953. These were obtained at the 0.9m telescope at Kitt Peak on the nights of 4-6 April 1999, with the T2KA 2048x2048 CCD camera in f/13.5 direct imaging mode. The integration time for the galaxies in  $\text{H}\alpha$  ranges from 360 to 420 seconds. The details of the data reduction for these galaxies are given in Sheth (2001). For NGC 3627, we use a K-band image from Regan & Elmegreen (1997).

### 3. Results

#### 3.1. (r) Galaxies

Figures 1, 2, and 3 show the BIMA SONG maps of velocity-integrated CO 1–0 emission for three of the galaxies classified as having inner rings compared with R band and  $\text{H}\alpha$  images at the same scale. Figures 1, 2, and 3 show that CO and  $\text{H}\alpha$  have similar distributions. The solid line indicates the 50% gain contour for the BIMA CO observations, showing the approximate field of view. The dashed line is an ellipse marking the approximate location of the inner ring. It is derived using the major axis size determined by de Vaucouleurs and Buta (1980), and adjusting the ellipse position angle and ellipticity to approximately match the inner ring seen in the R band and  $\text{H}\alpha$  images. The corresponding ellipse is also plotted in the CO images. CO emission coincident with the inner ring is detected in all three. Although the emission is faint ( $\sim 1 \text{ Jy beam}^{-1} \text{ km s}^{-1}$ ), it is clearly detected and has the expected galactic kinematic structure. In each galaxy, the CO emission also extends beyond the ring to larger radii, particularly in NGC 3953. The CO morphology alone could be described as a hole in the inner CO disk; it alone does not look very ring-like. On the other hand, only in NGC 3351 is emission detected inside of the ring. In this galaxy, bright emission near the nucleus and weaker emission in the inner bar region are detected. The central  $\text{H}\alpha$  emission is also brighter in this galaxy.

Inner ring CO emission is also detected in the other two (r) SONG galaxies, NGC 4725 and NGC 3726, neither of which are shown here (see Helfer et al. (2002)). For NGC 4725 the major axis diameter of the ring is  $260''$ , larger than the  $190''$  half-power BIMA mosaic

region. Consequently, the sensitivity at the expected location of the inner ring is poor; nonetheless, CO emission is detected coincident with the brighter optical arcs of the inner ring. The sensitivity is good within the bar region, but no CO is detected here, except near the nucleus. In NGC 3726, CO emission is detected from parts of the inner ring, but the relatively high inclination, small semi-minor axis of the inner ring ( $\sim 20''$ ), and presence of nuclear and bar dust lane CO emission make it difficult to clearly see the CO inner ring. Nonetheless, some CO emission coincident with the inner ring is detected.

The CO emission distribution for the five BIMA SONG galaxies classified as (r) is summarized in Table 1. The key finding is that CO emission coincident with the inner ring is detected in all five, but emission interior to the inner ring is not detected except near the nucleus.

### 3.2. (s) Galaxies

CO distributions for the seven SONG galaxies classified as spiral (s), indicating no inner ring, are summarized in the second part of Table 1 (images for all galaxies are shown in Helfer et al. (2002)). These include four with detected CO emission, but no obvious organized distribution: NGC 0925, NGC 2403, NGC 4258, and NGC 4490. The CO emission in NGC 0925 and NGC 2403 is weak; we note that these are classified as SABd and SABcd respectively, and are among the latest types in the SONG sample. The CO emission in NGC 4490 and NGC 4258 also has no clearly organized distribution but is significantly brighter; NGC 4490 is classified as a peculiar galaxy, and NGC 4258 is a well known disturbed galaxy (van der Kruit, Oort, & Mathewson 1972; Krause et al. 1990).

NGC 4535 has a CO emission distribution which at first glance appears to be an inner ring. Detailed inspection, however, shows that the CO coincides with the two spiral arms, which are very prominent and tightly wrapped in the optical. For NGC 4321, CO emission is detected essentially everywhere in the  $3'$  field of view, including the expected location of the inner ring. However, CO emission at the inner ring location is not enhanced, and for that reason we denote inner ring emission with a “?” in Table 1.

#### 3.2.1. NGC 3627

The detailed distribution of velocity-integrated CO emission is shown in Figure 4. The CO emission shows a peak at the nucleus, extends along the leading edges of the bar, forms two broad peaks at the bar ends, and then trails off into the spiral arms, with the western

arm emission extending over a greater distance.

The CO map also reveals additional weak emission extended roughly parallel to the bar but offset approximately  $20''$  both west and east of the bar. At its brightest, this emission is more than 10 times weaker than the emission at the bar ends. Although this emission is weak, it appears to be resolved, especially in the brighter western half of the ring. The deprojected ring is not obviously elongated. A deprojected image (e.g. Figure 3.7 in Sheth (2001)) shows that this emission lies along a circle or ring circumscribing the bar ends. It is this emission we identify as a molecular inner ring.

The inner ring is relatively weak compared to the nuclear and bar end emission. Such low level emission in the presence of bright emission in interferometric maps should be viewed with caution due to possible errors in the deconvolution. Consequently, we carefully examined the kinematic structure of the inner ring feature in order to evaluate whether this structure is in fact an inner ring.

For example, emission that extends over a large velocity range, as it does in the nucleus of NGC 3627, can appear in the velocity-integrated maps due to the accumulation of small errors in individual velocity channels. These errors leave a distinctive signature in the data because if the faint emission is due to the incomplete deconvolution of emission from a bright region, it will have velocity structure similar to the bright regions. Therefore, we can evaluate the weak features by investigating the morphology of the emission in the velocity cube.

In Figure 5(b) we show a long slit along the northwest section of the ring. Emission in the ring is from  $+5''$  to  $+35''$ . Similarly, we show a long slit along the southwest section of the ring in 5(c). Here emission in the ring is from  $-25''$  to  $0''$ . A comparison long slit along the bar and through the nucleus is shown in 5(a). The broad, bright emission from the nucleus is clear in the upper panel as is the bright emission from the bar ends. Clearly the ring emission is very narrow in its velocity extent and quite distinct kinematically from both the nucleus and the bar ends.

At this point we have shown that NGC 3627 exhibits CO emission resembling an inner ring, and the kinematic distribution indicates the emission is not an artifact. A further test as to whether the observed emission is in fact an inner ring is to compare the kinematics with that predicted by models of barred galaxies. Hydrodynamic models of gas flow in barred spirals have been successful at reproducing the kinematic signatures of gas flow in barred potentials (Regan, Vogel, & Teuben 1997; Regan, Sheth & Vogel 1999). In Figure 6 (right panel), we show a velocity map of NGC 3627 made by fitting Gaussian line profiles to the emission in the cube. We compare that to one generated from the models of Piner, Stone & Teuben (1995) (left panel), where the model has been smoothed to the resolution

of these observations, rotated, and scaled to match the orientation of NGC 3627 on the sky. The model is not expected to be an exact match to the observations because we used one of the standard Piner, Stone & Teuben (1995) models and did not attempt to match the gravitational potential of the observed galaxies. Also, the model does not include star formation, and thus the amount of gas at various positions will not match the observations (see discussion in Sheth et al. (2000)). The salient feature of the model is that, due to the orientations of the bar and the galaxy, gas in the western half of the inner ring is more red-shifted than gas directly to the east in the bar (except for the southern nuclear ring gas) or gas directly to the west further out in the disk; the observed data shows similarly that the western inner ring gas is more red-shifted than gas to the east or west. Emission from the western inner ring is weaker and its kinematics more difficult to discern. Note that these kinematics are also consistent with the model of the inner ring presented in Sakamoto, Baker, & Scoville (2000). In their model the inner ring was located at the approximate position of the UHR resonance.

Summarizing, we have found that although NGC 3627 is classified as an (s) galaxy, it has a ring of CO emission at the location expected for an inner ring, with kinematics consistent with that expected for an inner ring.

#### 4. Star Formation and Inner Rings

Our detection of a molecular inner ring in a galaxy previously classified as type (s) suggests that the fraction of galaxies with inner rings may be underestimated. As discussed in the Introduction, inner rings have been historically identified primarily due to star formation indicators, such as blue optical color excesses. The discovery of an inner ring using CO observations rather than  $H\alpha$  might suggest the existence of a population of inner rings in which the star formation efficiency (SFE) is lower. To test this, we can compare the SFE in the inner ring in the known (r) galaxies with that in NGC 3627. The SFE can be derived directly from the ratio of the  $H\alpha$  surface brightness to the CO surface brightness. The three (r) galaxies for which we have both resolved CO emission in the inner ring and calibrated  $H\alpha$  images are NGC 3344, NGC 3351, and NGC 3953 (shown in Figure 1). For each galaxy, we defined apertures that included the inner ring CO and  $H\alpha$  emission, and calculated the average surface brightnesses and ratios listed in Table 2. The apertures used for each region are shown in Figure 7. For NGC 3627, because the CO emission is not confined to the inner ring, we defined separate apertures for the inner ring, bar, bar end, and spiral arms. We did not include the bar ends in the region defined as the inner ring, since here the inner ring would be confused with the bright spiral arms. The Western and Eastern inner ring

measurements are listed in Table 2. Measurements for other regions in NGC 3627 are also listed.

Comparing the inner ring measurements listed in Table 2 we see that the SFE in NGC 3627 is actually the same as that in the galaxies classified as type (r). This implies that the optical classification of NGC 3627 as a type (s) galaxy cannot be attributed to a paucity of star formation or a lower SFE. Supporting this, Table 2 shows that the SFE is higher in the NGC 3627 inner ring than elsewhere in the galaxy. The low value in the nucleus might be attributed to dust extinction of  $H\alpha$  emission and enhanced CO emissivity. However, the higher SFE of the NGC 3627 ring compared to the other regions in the galaxy appears significant. A full investigation of how star formation efficiency varies in different regions in the BIMA SONG galaxies will be presented in Sheth, Thornley, Vogel, Regan, Wong (2002, in prep).

The fact that the inner ring in NGC 3627 does not show up as an excess of light in the K-band image may be an indication that the ring is quite young. If the interaction with NGC 3626 and NGC 3623 has only recently driven gas into the bar region, then the star formation in the inner ring may be quite recent and thus not yet had time to create the older stars that are seen in the near-infrared.

Why was NGC 3627 not identified as an (r) galaxy? It may be that the combination of relatively high inclination with the presence of star formation throughout the bar region makes the inner ring difficult to discern; in blue light the star formation and dust lanes within the inner ring would certainly reduce the contrast between the inner ring and the region interior to it. Also, de Vaucouleurs & Buta (1980) showed that the detection rate of inner rings decreased in high inclination galaxies. By contrast, in all the (r) galaxies shown here, in both CO and  $H\alpha$  there is a relatively well defined boundary interior to the radius of the inner ring. In these galaxies, the region swept by the bar has very little star formation (or CO), except near the nucleus, and so the inner ring is easily detected. In other words, it may be that inner rings are most readily *detected* in galaxies where the bar has swept most of the gas from the bar region into the nuclear region.

## 5. Summary

We have detected molecular inner rings in all five of the galaxies in the BIMA SONG previously classified as having an inner ring. In addition, we detect an inner ring in NGC 3627, a galaxy previously thought not to contain an inner ring. We propose that the large amount of star formation at the bar ends and along the bar of NGC 3627 combined with



the inclination of NGC 3627 reduced the contrast of the star formation in the inner ring and prevented an optical classification of this galaxy as having an inner ring.

The authors would like to thank the other members of the BIMA SONG team: Tamara Helfer, Michele Thornley, Tony Wong, Leo Blitz, Douglas Bock, and Andy Harris for their work on the observations and data reduction. We would also like to thank the comments of the anonymous referee for comments that improved the paper. This work is partially supported by NSF AST-9981289 and by the state of Maryland via support of the Laboratory for Millimeter-Wave Astronomy. KS acknowledges support from the NSF grant AST-9981546 which partially funds the Owens Valley Millimeter Array.

## REFERENCES

- Barth, A. J., Ho, L. C., Filippenko, A. V., Sargent, W. L. W. 1998, *ApJ*, 496, 133
- Buta, R. 1986, *ApJS*, 61, 609
- Buta, R., & Combes, F. 1996, *Fund. Cosmic Physics*, 17, 95.
- Buta, R. & Crocker, D. A. 1993, *AJ*, 105, 1344
- Buta, R. & de Vaucouleurs, G. 1983, *ApJS*, 51, 149
- Byrd, G., Rautiainen, P., Salo, H., Buta, R. & Crocker, D. A. 1994, *AJ*, 108, 476
- Combes, F. & Gerin, M. 1985, *A&A*, 150, 327
- de Vaucouleurs, G. & Buta, R. 1980, *AJ*, 85, 637
- Helfer, T. T., Thornley, M. D, Regan, M. W., Wong, T., Sheth, K., Vogel, S. N., Blitz, L., & Bock, D., C.-J. 2002, *ApJ*, in prep
- Kenney, J. D. P., Wilson, C. D., Scoville, N. Z., Devereux, N. A. & Young, J. S. 1992, *ApJ*, 395, L79
- Krause, M., Cox, P., Garcia-Barreto, J. A., & Downes, D. 1990, *A&A*, 233, L1
- Piner, B. G., Stone, J. M. & Teuben, P. J. 1995, *ApJ*, 449, 508
- Regan, M. W. & Elmegreen, D. M. 1997, *AJ*, 114, 965
- Regan, M. W., Sheth, K. & Vogel, S. N. 1999, *ApJ*, 526, 97
- Regan, M. W., Vogel, S. N., & Teuben, P. J. 1997, *ApJ*, 482, L143
- Regan, M. W., Thornley, M. D., Helfer, T. T., Sheth, K., Wong, T., Vogel, S. N., Blitz, L., & Bock, D., C.-J. 2001, *ApJ*, 561, 218
- Sakamoto, K., Okumura, S. K., Ishizuki, S. & Scoville, N. Z. 1999, *ApJ*, 525, 691
- Sakamoto, K., Baker, A. J., & Scoville, N. Z. 2000, *ApJ*, 533, 149
- Schwarz, M. P. 1984, *Proceedings of the Astronomical Society of Australia*, 5, 464
- Sheth, K. 2001, Ph. D. Dissertation, University of Maryland
- Sheth, K., Regan, M. W., Vogel, S. N. & Teuben, P. J. 2000, *ApJ*, 532, 221

van der Kruit, P. C., Oort, J. H., & Mathewson, D. S. 1972, *A&A*, 21, 169

Welch, W. J. et al. 1996, *PASP*, 108, 93

Table 1. CO Distribution in (r) and (s) SONG Barred Galaxies

| Galaxy                                       | Classification  | Nucleus | Bar<br>Dust lanes | Bar<br>Other | Inner<br>Ring | Spiral<br>Arms | Other |
|----------------------------------------------|-----------------|---------|-------------------|--------------|---------------|----------------|-------|
| Galaxies Classified as Inner Ring (Type (r)) |                 |         |                   |              |               |                |       |
| NGC 3344                                     | (R)SAB(r)bc     |         |                   |              | Y             | ?              |       |
| NGC 3351                                     | SB(r)b;HII      | Y       | I                 |              | Y             | ?              |       |
| NGC 3726                                     | SAB(r)c         | Y       | I                 | ?            | Y             | ?              |       |
| NGC 3953                                     | SB(r)bcHII/Lin  |         |                   |              | Y             | ?              |       |
| NGC 4725                                     | SAB(r)ab-pec Sy | Y       |                   |              | w             | ?              |       |
| Galaxies Classified as Spiral (Type (s))     |                 |         |                   |              |               |                |       |
| NGC 0925                                     | SAB(s)d         |         |                   |              |               |                | w     |
| NGC 2403                                     | SAB(s)cd        |         |                   |              |               |                | w     |
| NGC 3627                                     | SAB(s)b Sy      | Y       | Y                 | Y            | Y             | Y              |       |
| NGC 4258                                     | SAB(s)bc Sy1    |         |                   |              |               |                | Y     |
| NGC 4321                                     | SAB(s)bc HII    | Y       | Y                 | Y            | ?             | Y              |       |
| NGC 4490                                     | SAB(s)d pec     |         |                   |              |               |                | Y     |
| NGC 4535                                     | SAB(s)c         | Y       | Y                 |              |               | Y              |       |

Note. — A ? denotes the inability to determine if a feature exists. A “w” means weak and an “I” means inner bar dust lane

Table 2. Star Formation Efficiencies in Inner Rings

| Galaxy   | Region       | Area<br>kpc <sup>2</sup> | H $\alpha$ Flux<br>erg s <sup>-1</sup> cm <sup>-2</sup><br>(10 <sup>-13</sup> ) | CO Flux<br>Jy km s <sup>-1</sup> | SFR<br>M $_{\odot}$ yr <sup>-1</sup> | H <sub>2</sub> Mass<br>M $_{\odot}$<br>(10 <sup>7</sup> ) | SFR/H <sub>2</sub><br>Gyr <sup>-1</sup> |
|----------|--------------|--------------------------|---------------------------------------------------------------------------------|----------------------------------|--------------------------------------|-----------------------------------------------------------|-----------------------------------------|
| NGC 3344 | inner ring   | 9.8                      | 9.3                                                                             | 27                               | 0.38                                 | 4.6                                                       | 8.3                                     |
| NGC 3351 | inner ring   | 25.                      | 9.9                                                                             | 130                              | 0.26                                 | 15                                                        | 1.8                                     |
| NGC 3953 | inner ring   | 19                       | 2.3                                                                             | 156                              | 0.12                                 | 34                                                        | 0.36                                    |
| NGC 3627 | E inner ring | 2.6                      | 5.2                                                                             | 82                               | 0.17                                 | 11                                                        | 1.5                                     |
| NGC 3627 | W inner ring | 4.6                      | 3.5                                                                             | 118                              | 0.11                                 | 16                                                        | 0.71                                    |
| NGC 3627 | nucleus      | 0.7                      | 2.4                                                                             | 335                              | 0.078                                | 45                                                        | 0.17                                    |
| NGC 3627 | bar S        | 1.6                      | 2.6                                                                             | 196                              | 0.084                                | 26                                                        | 0.32                                    |
| NGC 3627 | bar N        | 1.5                      | 2.5                                                                             | 144                              | 0.082                                | 19                                                        | 0.42                                    |
| NGC 3627 | bar end S    | 1.2                      | 6.9                                                                             | 354                              | 0.23                                 | 48                                                        | 0.47                                    |
| NGC 3627 | bar end N    | 1.2                      | 8.2                                                                             | 304                              | 0.17                                 | 41                                                        | 0.65                                    |
| NGC 3627 | spiral arm S | 11.9                     | 12                                                                              | 596                              | 0.42                                 | 80                                                        | 0.52                                    |
| NGC 3627 | spiral arm N | 14.8                     | 9.1                                                                             | 691                              | 0.30                                 | 93                                                        | 0.32                                    |

Note. — The H<sub>2</sub> mass was found assuming the standard Galactic conversion from CO flux to H<sub>2</sub> mass.

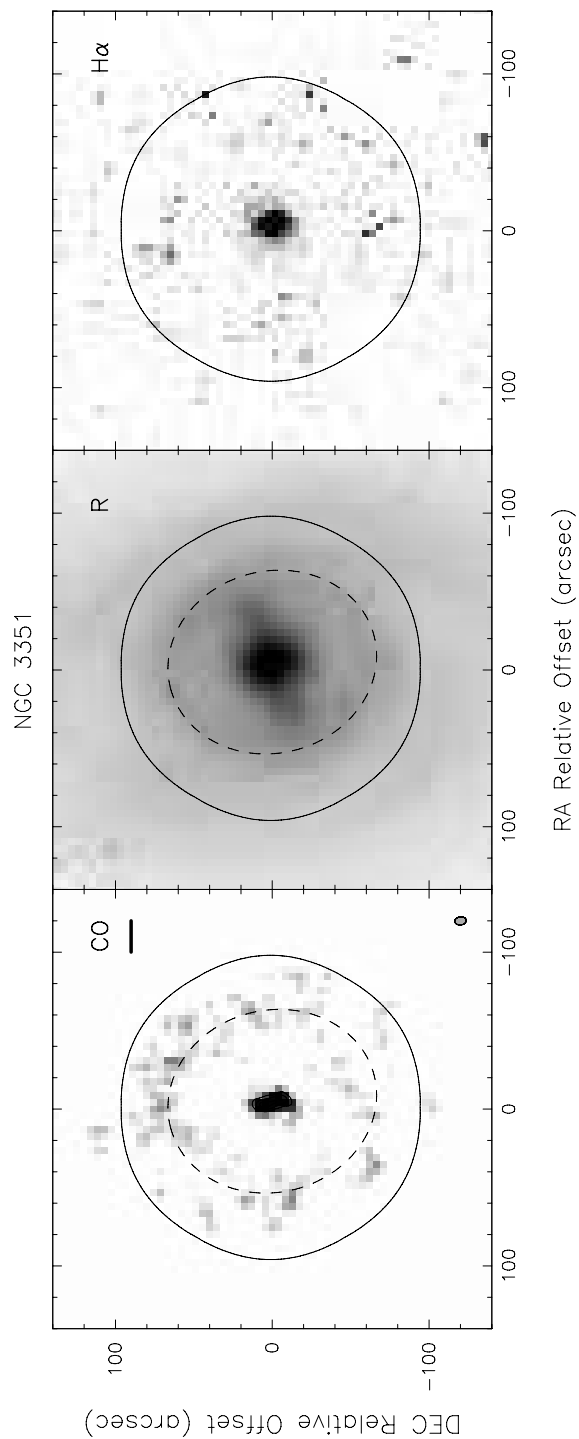


Fig. 1.— Comparison of CO 1–0 (left column), R-band (middle column), and  $H\alpha$  (right column) emission distribution for NGC 3344. The dashed ellipse indicates the location of the inner ring from de Vaucouleurs & Buta (1980). The solid line is the half-power contour of the BIMA CO mosaic. The size of the CO synthesized beam is shown as a filled ellipse in the lower right of each CO panel. The thick line in the upper right of each CO panel indicates a linear distance corresponding to 1 kpc.

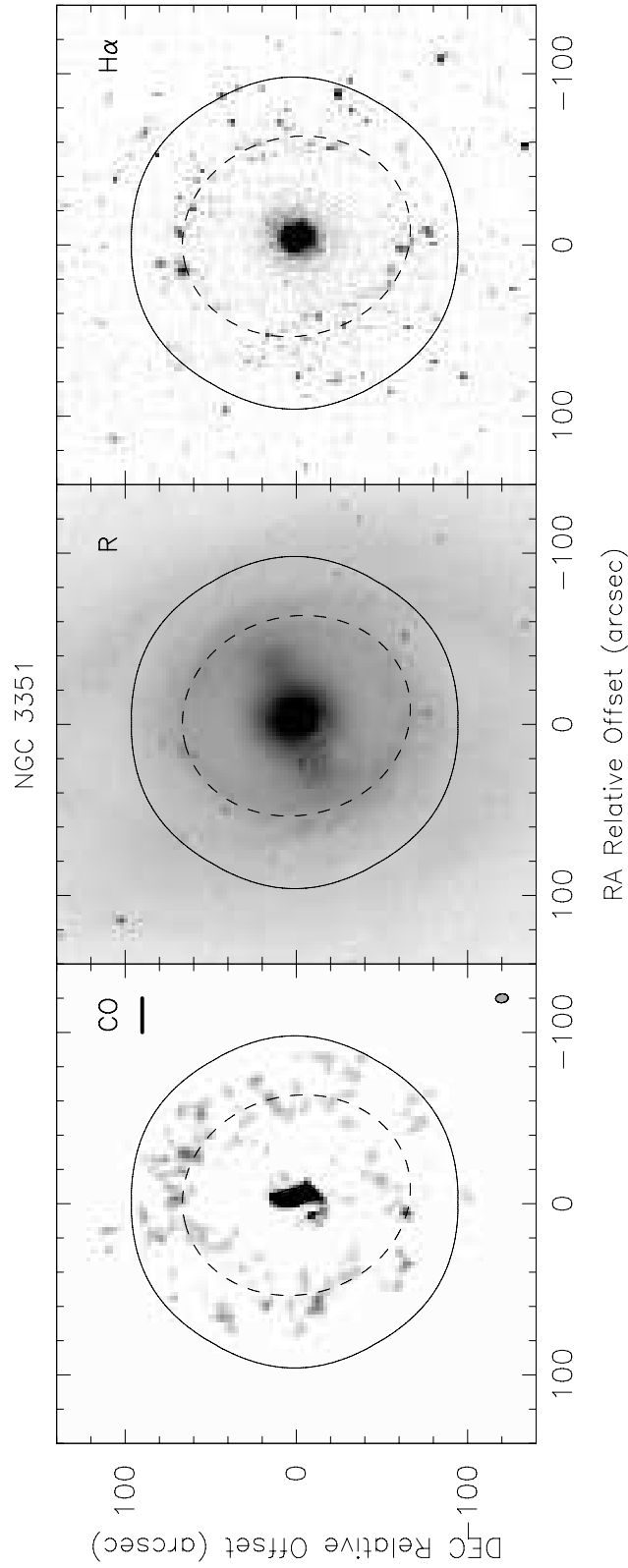


Fig. 2.— Comparison of CO 1–0 (left column), R-band (middle column), and H $\alpha$  (right column) emission distribution for NGC 3351. Otherwise the same as Figure 1.

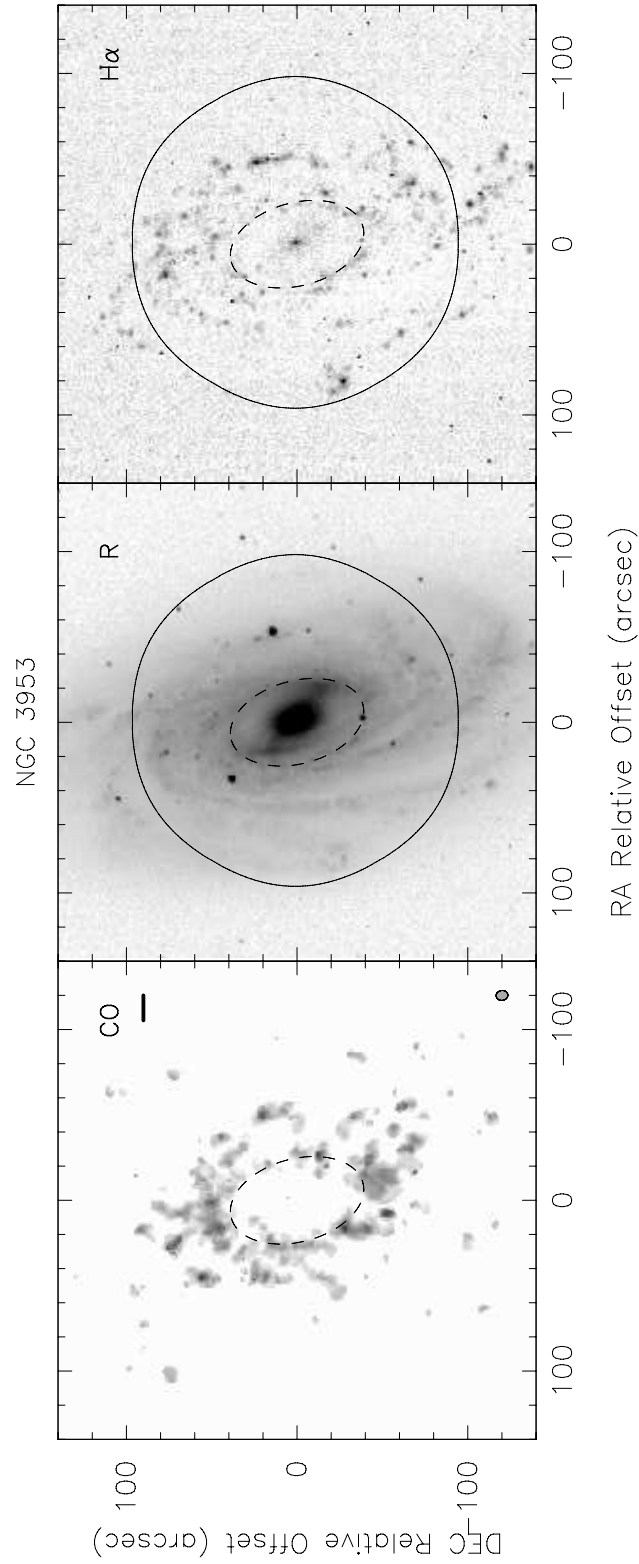


Fig. 3.— Comparison of CO 1–0 (left column), R-band (middle column), and H $\alpha$  (right column) emission distribution for NGC 3953(bottom). Otherwise the same as Figure 1.



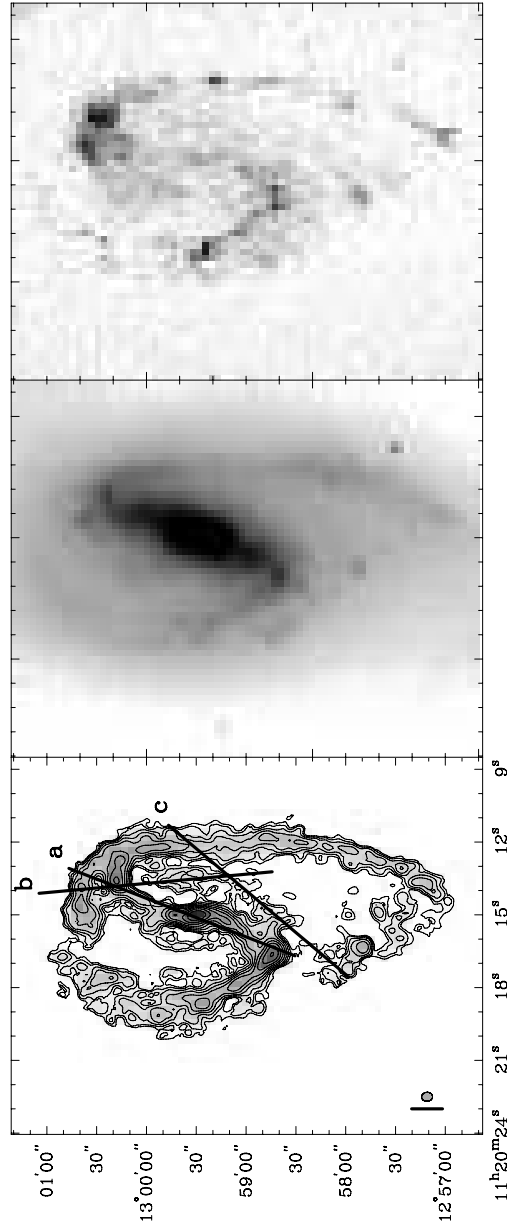


Fig. 4.— Left Panel) Velocity-integrated CO (1–0) emission distribution in NGC 3627, observed as part of the BIMA SONG. Contours begin at  $2.5 \text{ Jy km s}^{-1} \text{ beam}^{-1}$ , and are spaced at logarithmic intervals of 1.585. The vertical bar in the lower left corner shows 1 kpc at the assumed distance to NGC 3627 (11.1 Mpc). The synthesized beam is shown next to the vertical bar. The three lines show the positions of the long slits used to create Figure 5. Center Panel) A K-band image of NGC 3627 from Regan & Elmegreen (1997). The field of view is the same as the CO image. Right Panel) H  $\alpha$  emission in NGC 3627.

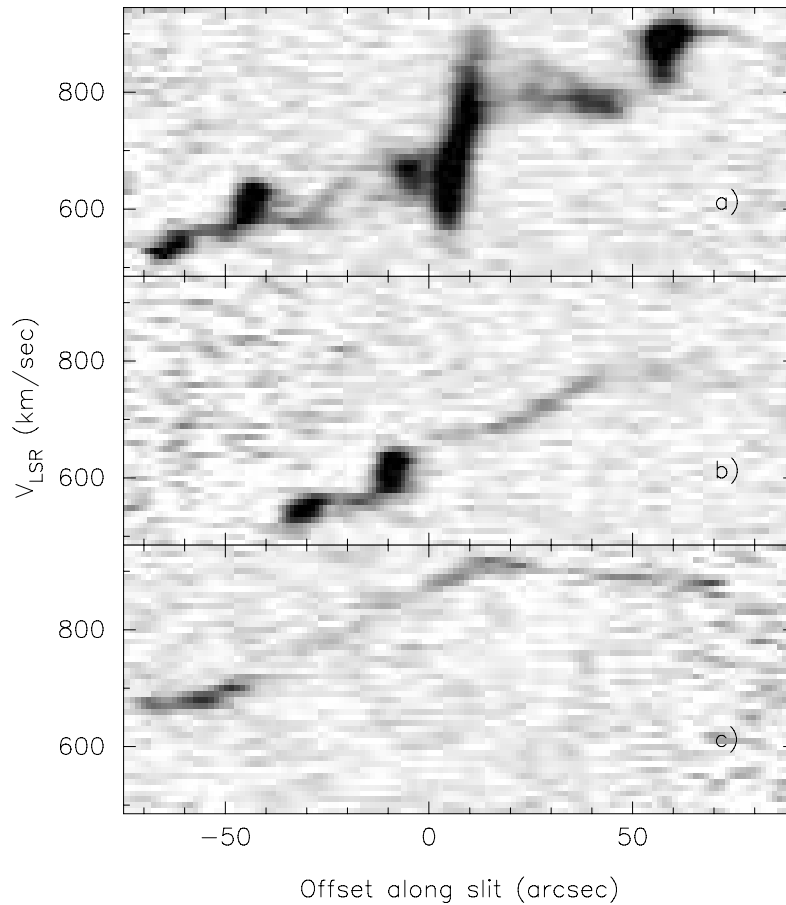


Fig. 5.— Position-velocity images of CO 1–0 emission in NGC 3627. Velocity is on the y axis, position along the “slit” on the x axis. a) A slit along the bar passing through the bright nuclear region. Bright emission from the northern bar end appear on the left. b) A slit along the northwestern section of the inner ring. The ring is at +5''(North) to +35''(South). c) A slit along the southwestern section of the inner ring. The ring is at -25''(North) to 0''(South). (See Figure 4 for the location of the slits). Comparing the inner ring emission with the bright emission, we see that the bar end is at a different velocity, and the nuclear region emission extends over a much broader velocity range.

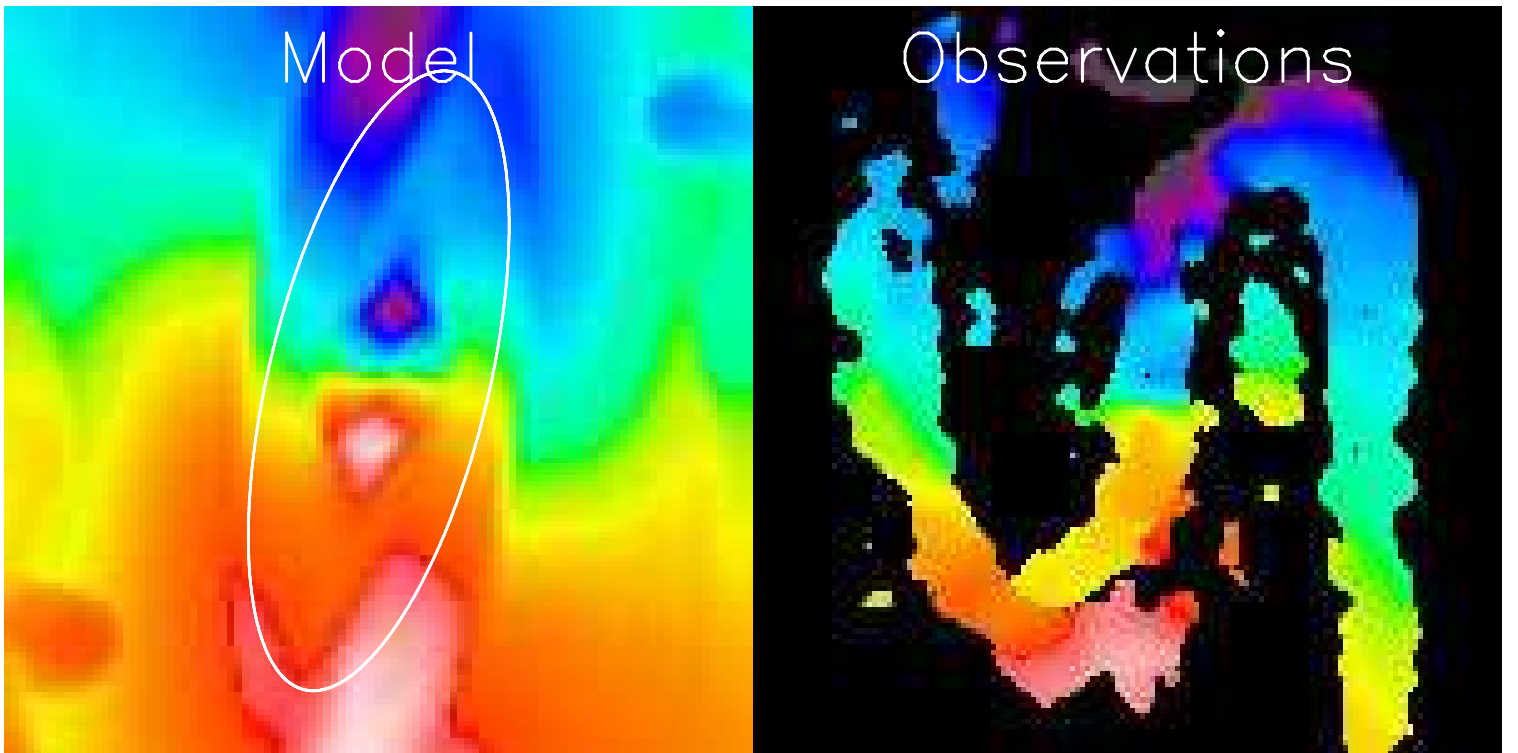


Fig. 6.— (Right panel) Velocities of CO emission observed for NGC 3627, derived from Gaussian fits to the line profiles. (Left panel) Velocities derived from the standard hydrodynamical model of Piner, Stone & Teuben (1995). The ellipse indicates the location of the inner ring.

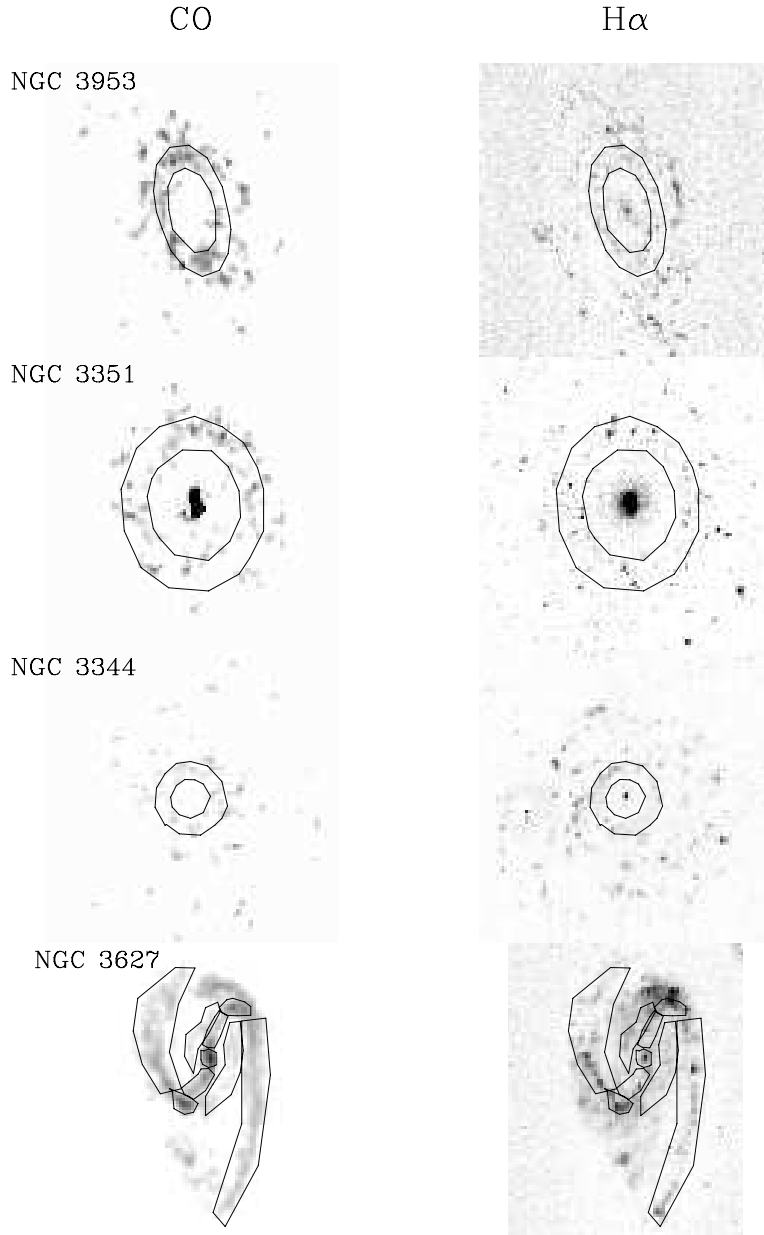


Fig. 7.— The various apertures used for the photometry. For NGC 3953, NGC 3351, and NGC 3344 the region used is an annulus. For NGC 3627 each of the various regions is defined by the drawn polygon.